Materials Science & Engineering A 558 (2012) 616–622

Contents lists available at SciVerse ScienceDirect

Materials Science & Engineering A

journal homepage: www.elsevier.com/locate/msea

Dependence of microstructure and mechanical properties on hot-extrusion temperatures of the developed high-strength Cu40Zn–CrFeTiSn brass by powder metallurgy

Shufeng Li [a,*], Hisashi Imai [a], Katsuyoshi Kondoh [a], Akimichi Kojima [b], Yoshiharu Kosaka [b], Koji Yamamoto [c], Motoi Takahashi [c]

[a] Joining and Welding Research Institute, Osaka University, 11-1 Mihogaoka, Ibaraki, Osaka 5670047, Japan
[b] San-Etsu Metals Co. Ltd., 1892, OHTA, Tonami, Toyama, Japan
[c] Nippon Atomized Metal Powders Corporation, 87-16 Nishi-Sangao, Noda, Chiba, Japan

ARTICLE INFO

Article history:
Received 16 April 2012
Received in revised form
10 August 2012
Accepted 14 August 2012
Available online 22 August 2012

Keywords:
Brass
Extrusion
Mechanical properties
Solid solution
Precipitation
Powder metallurgy

ABSTRACT

Effect of extrusion temperature on the microstructure and mechanical properties of the powder metallurgy Cu40Zn–CrFeTiSn alloy were investigated, through analysis on the solid solution of alloying elements, phase transformation and precipitation behavior. The extrusion was carried out between 500 °C and 650 °C using an extrusion ratio of 37:1. After extrusion, the microstructure was found consisting of the dual $\alpha+\beta$ phase structure and precipitates dispersing uniformly in the matrix. The tensile strength gradually decreased when the extrusion preheating temperature was increased. Solid solubility of Ti and Cr decreased steadily and grain coarsening occurred with increase in the extrusion temperature. Consequently, the lower extrusion preheating temperature was necessary to obtain excellent final mechanical properties, thus the extrusion temperature of 500 °C was enough to produce good ductility while maintaining the promising values of mechanical properties after extrusion.

1. Introduction

The widely used 60/40 brass is a dual phase alloy possessing the best combination of ductility and strength, these features enable 60/40 brass easily be casted to shape or fabricated by extrusion, rolling, drawing, hot stamping and cold forming. On the other hand, apart from the major alloying element Zn, small additions (less than 5 wt%) of other alloying elements are made to brasses to modify their properties for a given purpose [1], such as high strength, corrosion resistance, machinability and so on. In recent years, the impetus for the development of lead-free brasses and the development of the electronics industry has led to a number of new applications for brasses including lead frames, connectors and other electronic components [2,3]. These applications require brasses with unique combinations of mechanical strength and conductivity coupled with environment amiability. Solid solution strengthening and precipitation hardening are the primary methods used for developing high-strength brasses, by introducing alloying elements and impurities to improve the mechanical properties of brasses [4–6]. The binary phase diagrams of copper alloys [7] indicate that Cr, Fe, Ti, P, Co, Mg, Sn, etc. could be effectively used as candidate alloying elements for development of high-strength copper alloys. This is because the solid solubility of these alloying elements would decrease sharply with decreasing the temperature of copper. In order to obtain higher strength, more than one alloying elements are needed to form intermetallic precipitates, such as CrFe [8], Fe_2P [4], FeTi and Cu_4Ti [5], Cu_3Zr [6], etc. during aging process.

In powder metallurgy, it is possible to fabricate components which otherwise would decompose or disintegrate in direct alloying of melted materials. Powder processes are more flexible than casting and forging techniques, they are used in a wide range of industries, from automotive and aerospace applications to power tools and household appliances. The strengthening effect in conventional solid solution aging is limited due to low solubility of Cr, Fe and Ti in brass with coarse grain structure at the solid solution temperature. Rapid solidification in powder metallurgy process, e.g. high cooling rate can lead to supersaturated solid solution of Cr, Fe and Ti in brass matrix. Upon heat treatment, very fine dispersoids of second phase are precipitated in the matrix, as a result, the precipitation hardening effect is greatly enhanced. Additionally, during fabrication of high-strength brass alloys, powder-making process, consolidation and forming are the critical steps. The forming process after

* Corresponding author. Tel./fax: +81 6 6879 8669.
E-mail address: shufenglimail@gmail.com (S. Li).

0921-5093/$ - see front matter © 2012 Elsevier B.V. All rights reserved.
http://dx.doi.org/10.1016/j.msea.2012.08.062

consolidation is so complicated to be put under control, so it becomes the main factor that determines the final properties of the brass alloys. In order to obtain good mechanical properties, it should be taken into account that the super-saturated solid solution brass will decompose and the precipitates will coarsen during thermal histories in powder consolidation and hot extrusion. The purpose of the present paper is to investigate the effect of the extrusion temperature on microstructure and mechanical properties of the developed brass. Solid solution strengthening and precipitation hardening response of Cr, Fe and Ti alloying element additions on 60/40 brass matrix at different extrusion temperature are studied in detail.

2. Experimental

The nominal composition of Cu—40 wt%-Zn—0.7 wt%-Cr—0.2 wt%-Fe—0.6 wt%-Sn—0.6 wt%-Ti. (denoted as BS40-X) was designed as experimental alloy in the present research. The BS40-X brass alloy was prepared by melting the mixtures of pure Cu, Ti, Cr, Fe, Sn and Zn metals (>99.9 wt%) in an electrical induction furnace with an argon atmosphere and kept at 1673 K for several minutes to make the melt homogeneous. The molten alloy was poured into a heated tundish at 1673 K. In the water atomization process, high pressure water jet was directed against the molten stream to prepare rapidly solidified BS40-X alloy powder. The atomized powder was collected, dried and sieved. The chemical composition and particle size analysis were carried out, and the actual chemical composition was shown in Table 1.

As-atomized BS40-X brass powder was used as the raw material. 300 g powder was loaded into a cylindrical graphite die and consolidated by spark plasma sintering (DR.Sinter/SPS-1030; Sumitomo Coal Mining, Japan) at a pressure of 40 MPa under vacuum of 6 Pa. After sintered at 400 °C for 1.8 ks, the sample was cooled in the chamber to less than 150 °C. The obtained billet with diameter of 41 mm was extruded using hydraulic pressing with a load of 2000 kN (SHP-200-450; Shibayama Machine). For hot extrusion, the billets were preheated within the temperature range from 500 °C to 650 °C, stepping up the temperature every 50 °C in nitrogen gas atmosphere. The final diameter after extrusion was 7 mm. The extruded round bar was machined into tensile test sample with 3 mm diameter in accordance with ICS 59.100.01. Tensile test was conducted on a universal testing machine (Autograph AG-X 50 kN; Shimadzu) with a strain rate of $5\times10^{-4}\,s^{-1}$. The strain was recorded using a CCD camera accessorized to the machine. Three samples were prepared in identical conditions for the tensile strength test to obtain the average value. The schematic sketch of the water atomized powder procedure and the samples processing procedure are shown in Fig. 1.

The phase compositions in samples were identified by using X-ray diffraction (Labx, XRD-6100, Shimadzu) referenced to the standard ICDD PDF cards available in the system software. In addition, the microstructure evolution of the raw powder and samples were conducted by using a field-emission scan electronic microscope (FE-SEM, JEM-6500 F, JEOL), phases were examined by the energy-dispersive X-ray spectrometer (EDS) equipped by the SEM. Crystal orientation containing grain size and phase information was analyzed by electron backscatter diffraction (EBSD) technique, which was performed using TSL instrument attached to the FE-SEM operating at 20 kV. The longitudinal cross-section of the extruded sample was ground to 5 μm silicon carbide paper finish, and vibratory polished for 30 min to remove any remaining surface damage. The electron beam moved in 0.1 μm steps in an area 50 μm × 50 μm.

Table 1
Particle size and chemical composition of as-atomized BS40-X powder.

Powder	Particle size (μm)		mass (%)					
	Median size	Mean size	Zn	Cr	Fe	Sn	Ti	Cu
BS40-X	184.3	206.8	39.78	0.76	0.17	0.60	0.66	Bal.

3. Result and discussion

3.1. Characteristics of raw powder

The XRD pattern of the as-atomized powder sample was shown in Fig. 2. It clearly revealed that the powder contains mainly the β phase. The FE-SEM micrographs of the raw powder showed an irregular shape with a mean diameter of 206 μm as shown in Fig. 2(a), which was the typical morphology prepared by water-atomization process. The process resulted in the formation of super-saturated alloying elements in the matrix of β-brass phase through rapid solidification. Networks of small amount of ultrafine, nano-scale-sized precipitate particles existing along the grain boundaries were observed in the cross-section of the raw powder as shown in Fig. 2(b). The structure with tiny precipitate particles dispersed uniformly in matrix is expected to improve the properties of the extruded materials as it improves the grain refinement and is beneficial to work hardening.

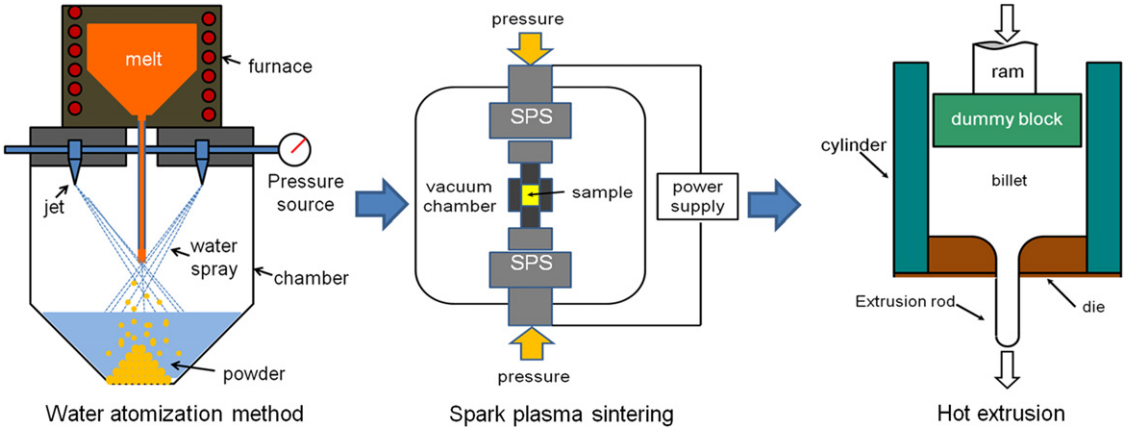

Fig. 1. Schematic sketch of experimental procedure used to prepare samples.

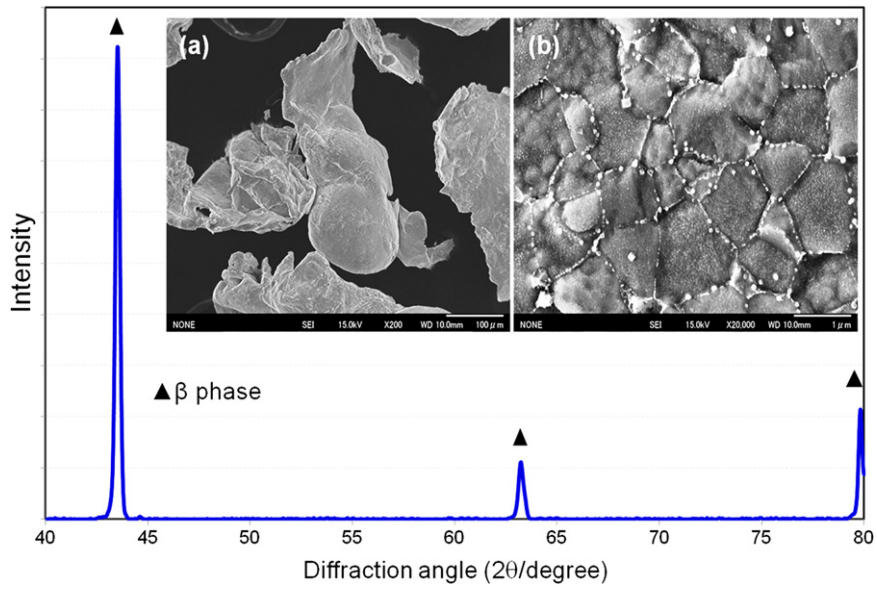

Fig. 2. XRD pattern and microstructure of as-atomized BS40-X raw powder. (a) Morphology of raw powder, and (b) cross-section of raw powder.

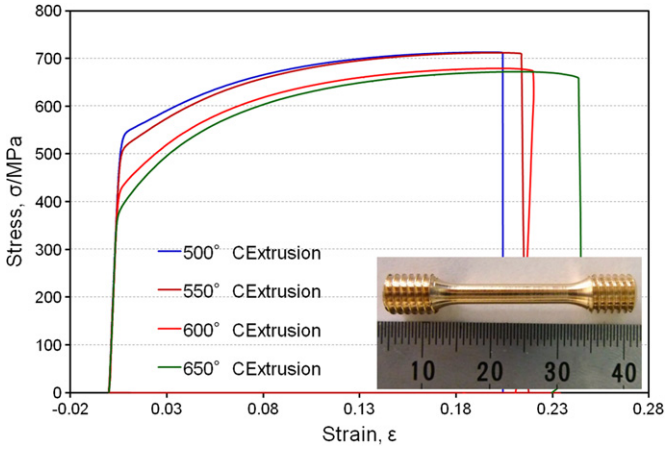

Fig. 3. True stress–strain curves of extruded BS40-X alloy at different extrusion temperature.

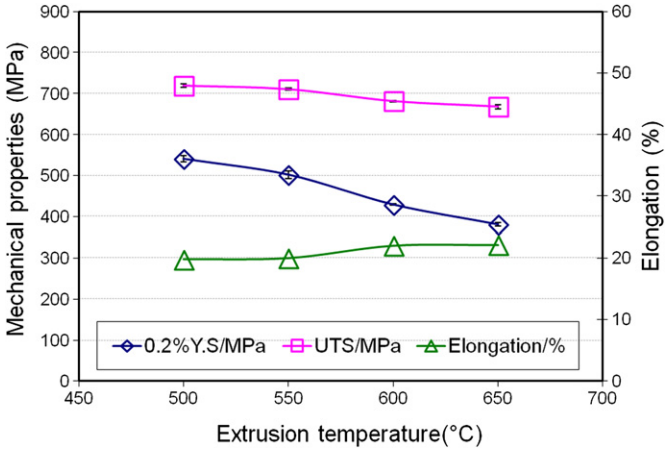

Fig. 4. Tensile properties of extruded BS40-X alloy as a function of extrusion temperature.

3.2. Mechanical properties

Fig. 3 presented the true strain–stress curves of the extruded BS40-X alloy at different extrusion temperature. A photograph of the tensile sample used to evaluate the mechanical properties was presented in Fig. 3. The results of the tensile properties have been summarized in Table 1. Accordingly, the dependence of tensile properties on the extrusion temperatures was plotted in Fig. 4. The yield strength (σ_{YS}) and tensile strength (σ_{UTS}) showed higher values at the lower extrusion temperature, saying, σ_{YS} was 540 MPa and σ_{UTS} was 719 MPa when it was extruded at 500 °C. The variations tendency of the yield and tensile strength were continue to decline when the extrusion temperature was increased. The higher tensile strength at lower extrusion temperature could be attributed to the strain hardening that occurred during plastic deformation in the extrusion process, which was increased in the case of extrusion at lower temperature. This led to the formation of finer microstructure that finally contributed to the improvement in the mechanical properties. It could also be shown from Fig. 4 that the elongation of the sample extruded at higher temperature showed limited improvement, from 19.8% at 500 °C increased to 22.1% at 650 °C. This result showed that the extrusion temperature at 500 °C was enough to produce good bonding between BS40-X powder particles after extrusion while maintained promising values of mechanical properties (Table 2).

Table 2
Tensile properties of extruded BS40-X alloy at different extrusion temperature.

Temperature (°C)	YS (MPa)	Deviation	UTS (MPa)	Deviation	Elongation (%)	Deviation
500	540.4	7.4	719.2	4.9	19.8	0.6
550	502.0	8.9	710.4	2.1	19.9	2.5
600	429.5	1.6	681.2	1.4	22.0	1.7
650	381.2	3.8	667.6	5.3	22.1	1.9

3.3. Microstructures of extruded materials

Fig. 5 showed the observed FE-SEM microstructure of BS40-X compact sintered at 400 °C using SPS. The raw powders were produced by water atomization consisted of fundamentally equiaxed grains of the β' phase as shown in Fig. 2(b). After sintering at 400 °C, the α phase was observed to distribute along

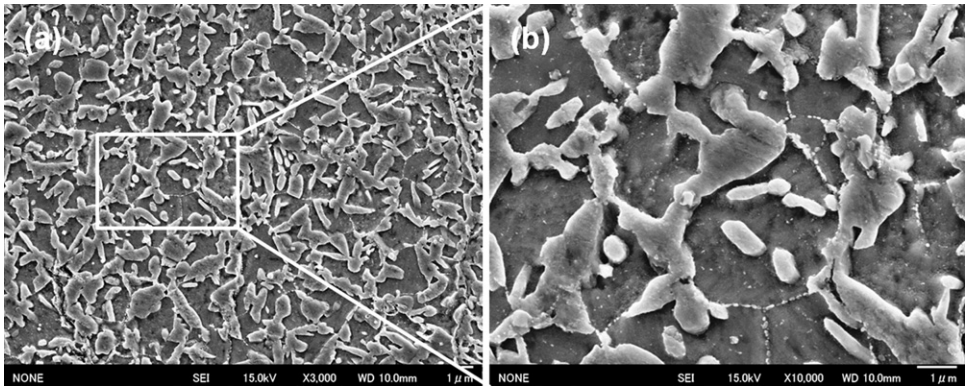

Fig. 5. FE-SEM microstructure of SPS compact. (a) x3000, (b) x10,000.

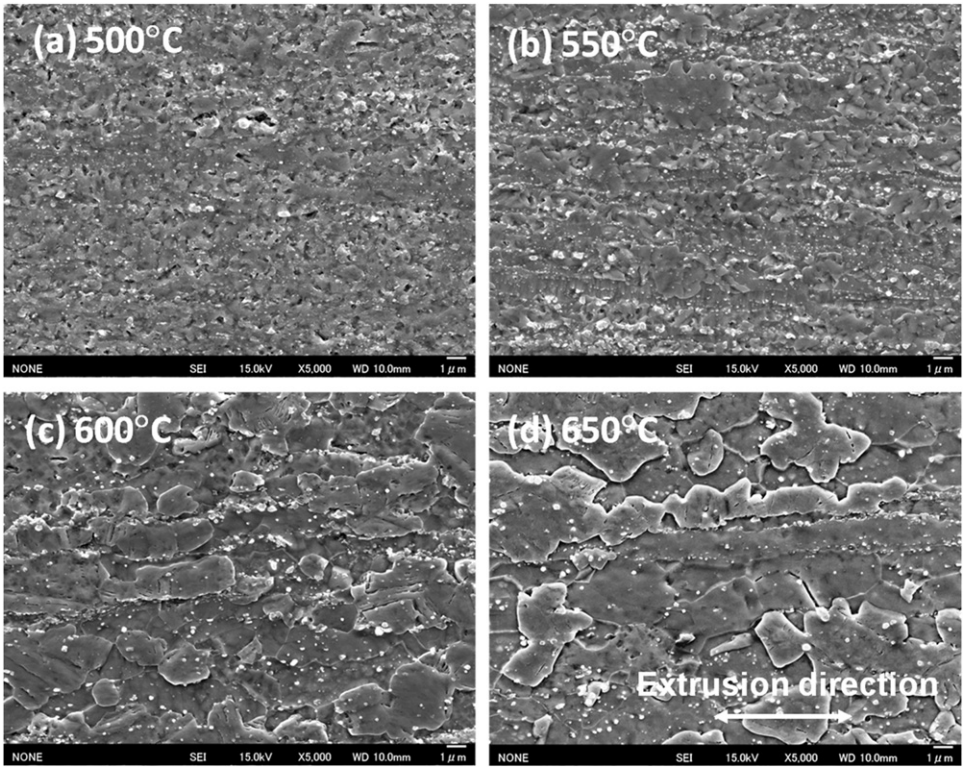

Fig. 6. Microstructures of extruded BS40-X samples along extrusion direction within temperature range from 500 °C to 650 °C.

the boundaries of the initial β' phase, which was surrounded by a matrix of deeper etching β' phase in Fig. 5(b).

Fig. 6 showed the microstructure of BS40-X brass extruded within temperature range from 500 °C to 650 °C. Generally, the powder produced by water atomization could result in very fine and uniform grain sizes in the order of 0.5∼1.0 μm as shown in Fig. 2(b). In the case of wrought brass with an extrusion ratio of 37 at 500 °C, a microstructure of minute recrystallized grains was obtained. The α phase is hardly to be distinguished from β phase matrix (Fig. 6(a)). Ultrafine precipitate particles were uniformly dispersed throughout the structure. Such a microstructure is expected to be helpful in increasing the mechanical properties of brass alloys. The samples extruded at 600 °C and 650 °C showed quite different morphology from the sample extruded at lower temperatures (Fig. 6(c)). The α phase became progressively coarse and elongates along the extrusion direction. Additionally, the precipitate particles grew coarser and distributed along the plastic flow line between the α/β-phase bands. This microstructure was explained by the tendency of precipitates to segregate at the primary particle boundaries when the green compact was preheated at higher temperature, which consequently weakened the constraints of the grain growth by precipitates [9]. Precipitates were redistributed with the flow of the large plastic deformation of the soft brass matrix by the high extrusion pressure during the subsequent hot extrusion. Fig. 7(a and b) depicted the TEM micrographs of the BS40-X compact sintered at 400 °C by SPS. Precipitate particles with a size of 50 nm were observed in the interiors of grains and at grain boundaries, as shown in the bright field (BF) image of Fig. 7(a). These precipitates were also discernible in the dark-field (DF) image of Fig. 7(b).

The atom concentration variations of the alloying elements in α phase and β phase after extruded at different temperature were shown in Fig. 8. It could be seen that atom concentrations of Ti

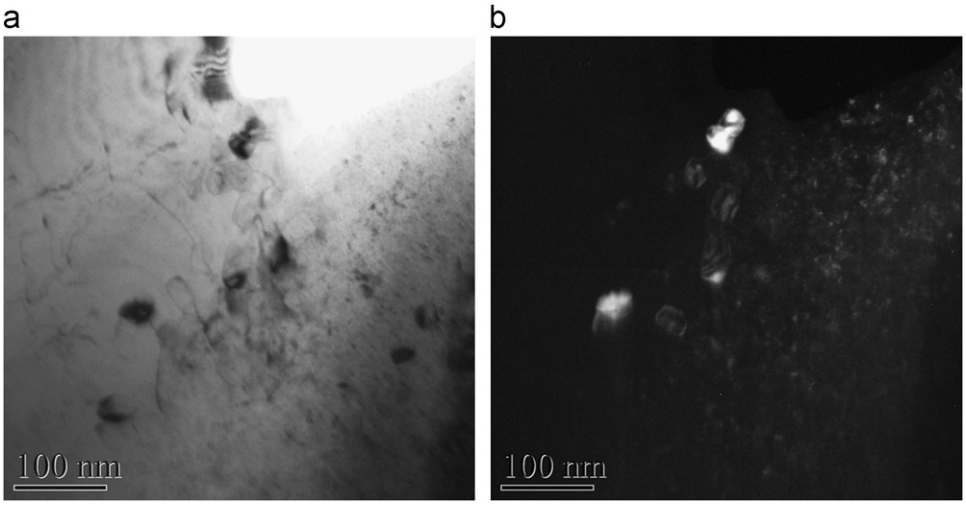

Fig. 7. Transmission electron micrographs of extruded BS40-X alloy consolidated at 500 °C by SPS (a) bright-field image; (b) dark-field image.

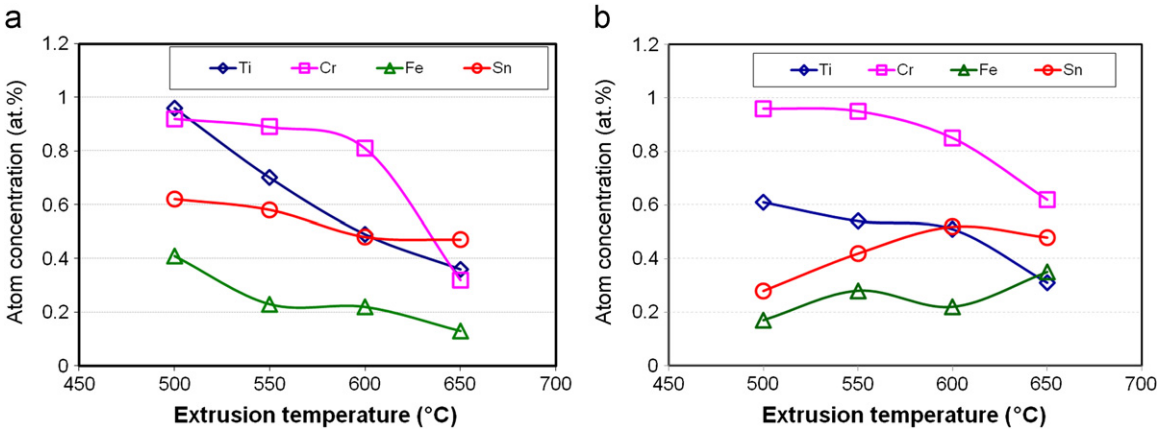

Fig. 8. Atom concentrations of alloying elements in (a) alpha phase and (b) beta phase as functions of extrusion temperature.

and Cr in α phase decreased steadily with increase of extrusion temperature, as well as in β phase. It was reported that the maximum solubility of Ti in copper is 8.0 at% at 885 °C, while at room temperature the solubility is < 1.0 at% [10]. The maximum solubility of Ti in Zn is 0.027 at% at room temperature [11]. It implies the equilibrium solid solubility of Ti in Cu40Zn brass less than that of Ti in copper. As for the results at present study, when the preheating temperature of the billet was 500 °C, the atom concentration of Ti in α phase and β phase were 0.96 at% and 0.61 at%, and their values decreased to 0.36 at% and 0.31 at% as preheat temperature increased to 650 °C. At the same time, the atom concentration of Cr continuously decreased when extrusion preheat temperature was increased. Especially, Cr concentration dropped off dramatically in both α and β phase when temperature was over 550 °C. Cu–Cr alloys have a large precipitation hardening response because the super- saturation of Cr in the Cu matrix creates a high degree of thermo-dynamic meta-stability in the solution treated condition, thus providing a high chemical potential for the precipitation reaction of Cr [8,12]. Atom concentrations of Sn and Fe in α phase continued to decline when extrusion temperature was increased. However, a contrary tendency was observed in β phase for variations of atom concentration of Sn and Fe.

Fig. 9 presented the image quality (IQ) map of the longitudinal cross-section micrographs of the extruded BS40-X as detected by the EBSD (electron backscatter diffraction) technique. The grain boundaries were identified by the lines, and the phase boundaries were identified by colors. The green area represented α-phase grains, and the red area represented β-phase grains. At the lower extrusion temperatures, the α phase was defined as fine globules distributed along a different band after extrusion. Recrystallization occurred in both the α phase and the β phase after hot extrusion, and the β phase exhibited a much finer grain size than does the α phase. Twins could be observed in the α phase, which are a typical feature for dual brass (Fig. 9(a)). Grains in both the α and β phases grew moderately at 500 °C. The precipitate particles (black dots) appeared as tiny second particles not only dispersed along the plastic flow line between α/β phase bands, but also dispersed in grain boundaries (Fig. 9(b)). The morphology of the extrusion sample at 600 °C and 650 °C differed from the morphologies of samples extruded at lower temperatures. The α phase became coarser and elongated successively along the extrusion direction (Fig. 9(c and d)).

Phase volume fraction in the samples detected by EBSD phase analysis was plotted as a function of extrusion temperature (Fig. 10). The volume fraction of α phase decreases from 52% to 49% as the extrusion temperature increases from 500 °C to 650 °C. The α phase volume fraction has an maximum value of 52% at 500 °C, which also accorded with the Cu–Zn binary phase diagram [2]. The volume fraction of β phase showed corresponding

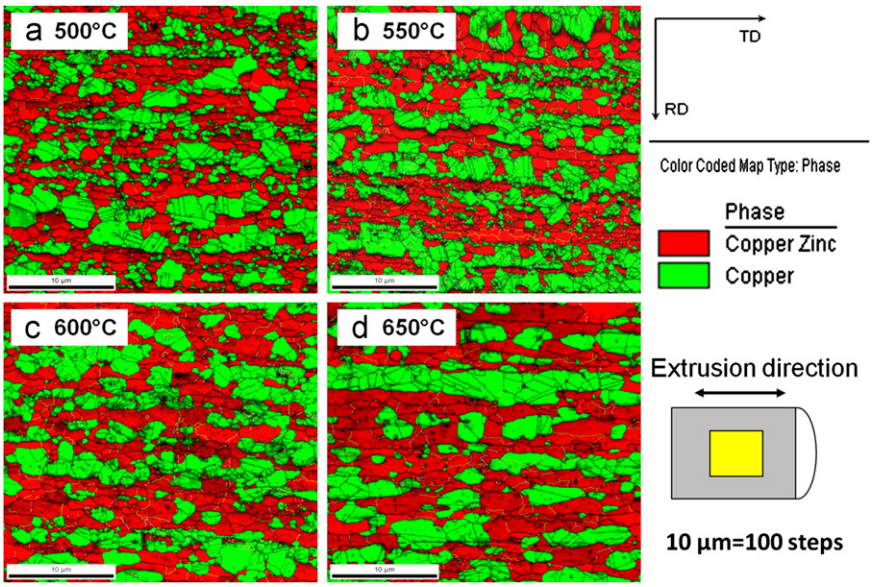

Fig. 9. Image quality (IQ) map of longitudinal cross-section of extruded BS40-X alloy at different extrusion temperature.

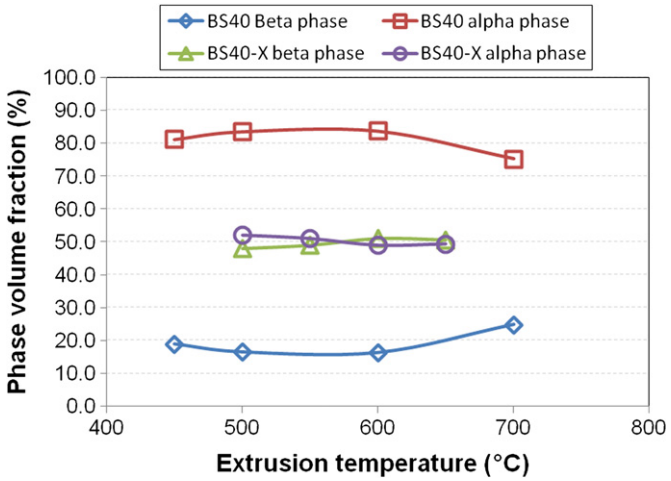

Fig. 10. Phase volume fractions in extruded BS40-X and BS40 brasses as functions of extrusion temperature.

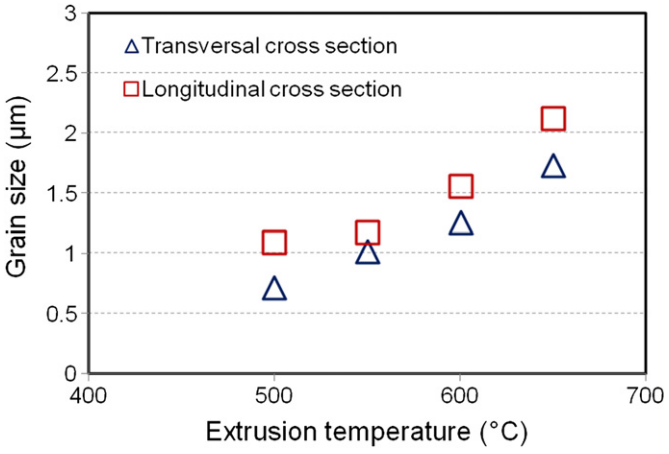

Fig. 11. Grain size in longitudinal and transversal directions of extruded BS40-X alloy as function of extrusion temperature.

balance variation with that of α phase: increased from 48% to 51% within temperature range of 500 °C–650 °C. The increase volume fraction of the harder β phase is effective to enhance the mechanical strength in dual phase brass [13]. However, because of the less variation ranges 3% in phase ratio, the limited effects of phase volume fraction on tensile strength at different extrusion temperature could be observed at present conditions. Compared with the phase volume fraction of BS40, BS40-X showed much higher β phase ratio because of alloying elements such as Sn can significantly increase the β phase ratio.

The grain sizes in the longitudinal and transversal directions of the extruded samples as functions of extrusion temperature within range of 500 °C–650 °C were plotted in Fig. 11. The sample extruded at lower temperature exhibited much smaller grain size than does the sample extruded at higher temperature in both of the longitudinal and transversal extrusion directions. According to the grain size in the longitudinal direction of the extruded samples detected by EBSD, the relationship curves between YS and grain size, the so-called Hall–Petch relationship curves were plotted in Fig. 12. The correlation between YS and grain size for the extruded BS40-X showed good linear-fit relationship, that is

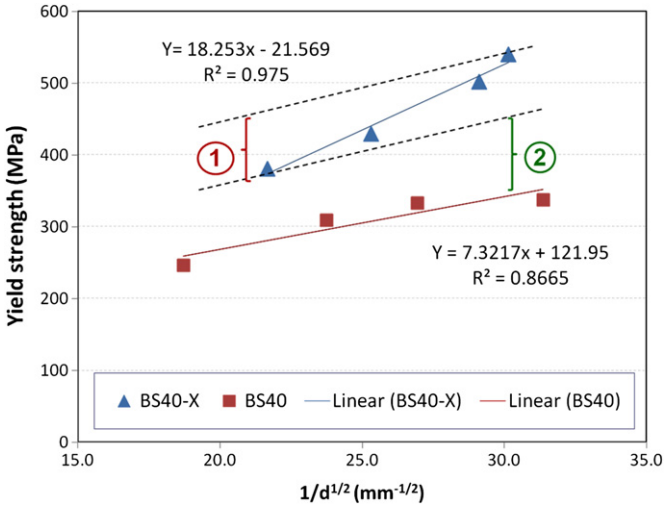

Fig. 12. Hall–Petch relationship between yield strength and grain size in the longitudinal direction of extruded BS40-X brass at different extrusion temperature.

to say, the yield strength of BS40-X brass increased with reduction in grain size. On the other hand, compared to that of BS40, BS40-X brass showed higher slope value, which means that BS40-X brass illustrates higher strengthening effect. YS of 540 MPa and UTS of 719 MPa for BS40-X after extruded at 500 °C showed 62.7% and 45.3% higher values than that of 60/40 brass. The strengthening effect decreased 84 MPa (part 1) with increasing extrusion temperature, which from the decrease of atom concentrations of Cr and Ti with increase of extrusion temperature from 500 °C to 650 °C. In addition, BS40-X extruded at 650 °C retained 80 MPa (part 2) higher yield strength than that of BS40, this strengthening value resulted from the higher β phase ratio and remained solid solutions of Cr, Fe, Ti and Sn after extruded at 650 °C.

3.4. Discussion

From a viewpoint of the alloy design and materials processing, the difference in atomic radii between Ti, Cr, Fe, Sn, Cu, and Zn provides a strain field, which is favorable for the solid solution strengthening. A high cooling rate can lead to the formation of a more refined microstructure, extend the solid solubility and even result in meta-stable phases [14,15]. Rapid solidification retains the single β' phase, and the super-saturated solid solution of Cr, Fe and Ti in BS40-X raw powder is formed. Virtually insoluble Cr and Ti show large precipitation-hardening response in 60/40 brass matrix, because of the super-saturation of Ti and Cr in the 60/40 brass matrix creates a high degree of thermo-dynamic meta-stability. This meta-stability provides a high chemical potential for the precipitation reaction of Ti and Cr in 60/40 brass. As cooling down from the high temperature during powder consolidation or forming, solid solution of Ti and Cr in brass decreases rapidly and presents in form of fine precipitates.

Rapid cooling from high temperatures is one method for applying stress to cause dislocation motion [16] and increase atomic vacancies thereby creating a high precipitation potential in the raw powder. The higher dislocation density and atomic vacancies provide more sites for precipitation, which provide a thermo-kinetic advantage for the precipitation reaction [17]. Super-saturated solution of Cr and Ti in the brass matrix creates a high chemical potential for the precipitation reaction. Additionally, the dislocation density increases gradually with increasing deformation strain during hot extrusion, which supplies more potential nucleation sites for Cr and Ti precipitation. The precipitates distribute in grain boundaries and act as a pinning effect, which increase resistance to grain boundary slip and produce marked work-hardening effects. As a result, BS40-X exhibits significantly stronger mechanical properties at low extrusion temperature than that of 60/40 brass.

A higher preheating temperature is appreciated with regard to the process of the materials, that is to say, rising the preheating temperature can decrease the deformation resistance during hot-extrusion. However, the rise of the preheating temperature will result in the ripening of the precipitates. The precipitate ripening rate (dr/dt) is given as follows [18]:

$$dr/dt = Dc\sigma r^{-2} \quad (1)$$

where r is the precipitate size; dr/dt is the interfacial energy between the matrix and the precipitate; c is the equilibrium solubility. According to the above relation, the increase of the diffusion coefficient D and the equilibrium solubility c due to the increase of the temperature will lead to the increase the precipitate ripening rate and the degradation of the mechanical properties of the alloys. It is appreciated that a lower preheating temperature is necessary for excellent properties of the wrought alloys.

Additionally, the possible recovery or dynamic recrystallization induced by hot deformation at higher temperatures might reduce the dislocation density [19,20]. The recrystallization that occurs after hot-extrusion decreases the dislocation density, which strongly affects the mechanical behaviors of BS40-X. Consequently, the mechanical properties of BS40-X continue to weaken due to the coarsening and clearing away of Ti and Cr precipitates in the grain boundaries at elevated extrusion temperatures.

4. Conclusion

The microstructure, phase-transformation behavior, precipitation behavior and mechanical properties of BS40-X brass were studied at different extrusion temperature by powder metallurgy processing.

(1) Super-saturated solid solution of Cr, Fe and Ti in water-atomized 60/40 brass powder created a high chemical potential for the precipitation reaction. Atom concentrations of Ti and Cr reduced rapidly by increasing the extrusion temperature, Ti and Cr elements presented in form of fine precipitates in the brass matrix, the ripening of the precipitates consequently weakened the constraints of the grain growth, thus resulted in degrade of mechanical properties by decrease of solid solution and grain growth as rise of extrusion preheating temperature.
(2) The lower extrusion preheating temperature is necessary to obtain the excellent final mechanical properties, thus the extrusion temperature at 500 °C was enough to produce good ductility after extrusion while maintaining the promising values of mechanical properties.

Acknowledgment

This work was supported as a project of the Japan Science and Technology Agency (JST). The authors sincerely thank the researchers of the Joining and Welding Research Institute (JWRI) at Osaka University as well as Mr. Yoshinori Muraki and Mr. Kyugo Inui for assistance in carrying out the extrusion experiments and tensile tests.

References

[1] S.W. Fortune, Structure and properties of engineering alloys, second ed., McGraw-Hill, 1993, p. 243.
[2] Metals Handbook, desk edition, ASM, Ohio, USA, 1984, p. 71.
[3] J.R. Davis, Alloying, Understanding The Basics, ASM International, Materials Park, OH 44073-0002, 2005.
[4] De-ping Lu, Jun Wang, Wei-jun Zeng, Yong Liu, Lei Lu, Bao-de Sun, Mater. Sci. Eng. A 421 (2006) 254–259.
[5] T.K. Vaidyanathan, K. Mukherjee, Mater. Sci. Eng. 24 (1976) 143–152.
[6] Ping Liu, Juanhua Su, Qiming Dong, Hejun Li, J. Mater. Sci. Tech. 21 (2005) 475–478.
[7] Metals Handbook, Alloy Phase Diagrams, ASM Handbook, vol. 3, 10th ed., 1990.
[8] H. Fernee, J. Nairn, A. Atrens, J. Mater. Sci. 36 (2001) 5497–5510.
[9] Shufeng Li, Hisashi Imai, Haruhiko Atsumi, Katsuyoshi Kondoh, Akimichi Kojima, Yoshiharu Kosaka, Koji Yamamoto, Motoi Takahashi, Mater. Sci. Eng. A 535 (2012) 22–31.
[10] Binary Alloy Phase Diagrams, Metals Handbook, vol. 1, ASM, Metals Park, OH, 1986, p.820.
[11] J.L. Murray, Phase Diagram of Binary Titanium Alloys, ASM International, 1987.
[12] A. Artens, J. Nairn, H. Fernee, G. Skennerton, A. Olofinjana., Mater. Forum 21 (1997) 57.
[13] J.R. Davis, Copper and Copper Alloys, in: Handbook Committee, ASM International, Materials Park, OH 44073-0002, 2001.
[14] H. Jones, Mater. Lett. 26 (1996) 133–136.
[15] L. Katgerman, F. Dom, Mater. Sci. Eng. A 375–377 (2004) 1212–1216.
[16] J.W. Hall, H.F. Rase, Ind. Eng. Chem. Fund. 3 (1964) 158–167.
[17] K.C.H. Kumar, I. Ansara, P. Wollants, L. Delaey, Z. Metallkd. 87 (1996) 666–672.
[18] Shigenori Yamauchi, Kazuhisa Shibue, Development of elevated temperature P/M aluminium alloy by rapid solidification processing, Sumitomo Light M. Tec. 29 (10) (1988) 250–256.
[19] W. Mao, Z. An, Y. Li, Front. Mater. Sci. China 2 (2008) 233.
[20] W. Mao, Z. An, W. Guo, P. Yang, Steel Res. Int. 81 (2010) 6.